

Article

Generation of Energetic Highly Elliptical Extreme Ultraviolet Radiation

Emmanouil Vassakis^{1,2}, Ioannis Orfanos¹ , Ioannis Liontos¹  and Emmanouil Skantzakis^{1,*} 

¹ Foundation for Research and Technology—Hellas, Institute of Electronic Structure & Laser, P.O. Box 1527, GR71110 Heraklion, Crete, Greece; evassakis@iesl.forth.gr (E.V.); orfanos@iesl.forth.gr (I.O.); iliontos@iesl.forth.gr (I.L.)

² Department of Physics, University of Crete, P.O. Box 2208, GR71003 Heraklion, Crete, Greece

* Correspondence: skanman@iesl.forth.gr

Abstract: In this study, the generation of energetic coherent extreme ultraviolet (XUV) radiation with the potential for controlled polarization is reported. The XUV radiation results from the process of high harmonic generation (HHG) in a gas phase atomic medium, driven by an intense two-color circularly polarized counter-rotating laser field, under loose focusing geometry conditions. The energy of the XUV radiation emitted per laser pulse is found to be of the order of ~100 nJ with the spectrum spanning from 17 to 26 eV. The demonstrated energy values (along with tight XUV focusing geometries) are sufficient to induce nonlinear processes. Our results challenge current perspectives regarding ultrafast investigations of chiral phenomena in the XUV spectral region.

Keywords: high harmonic generation; highly elliptical XUV radiation; energetic XUV pulses



Citation: Vassakis, E.; Orfanos, I.; Liontos, I.; Skantzakis, E. Generation of Energetic Highly Elliptical Extreme Ultraviolet Radiation. *Photonics* **2021**, *8*, 378. <https://doi.org/10.3390/photonics8090378>

Received: 6 July 2021

Accepted: 6 September 2021

Published: 9 September 2021

Publisher's Note: MDPI stays neutral with regard to jurisdictional claims in published maps and institutional affiliations.



Copyright: © 2021 by the authors. Licensee MDPI, Basel, Switzerland. This article is an open access article distributed under the terms and conditions of the Creative Commons Attribution (CC BY) license (<https://creativecommons.org/licenses/by/4.0/>).

1. Introduction

Coherent XUV laser-driven sources based on HHG processes have been extensively explored and used for a variety of applications in ultrafast science [1–17]. Furthermore, many HHG-based experimental strategies have been implemented in the production and characterization of intense attosecond light sources [15,18–28]. However, these pulsed sources, which are typically bright enough to induce non-linear processes and temporally short enough to map electronic motion, are mostly limited to emit only linearly polarized radiation (being driven by linearly polarized fundamental laser fields). Circularly polarized (CP) XUV light pulses have proven to be a valuable tool and have attracted a keen interest in the scientific community for a broad range of investigations such as chirality-sensitive light-matter interactions, angle-resolved photoemission spectroscopy, and magnetic circular dichroism spectroscopy. Novel approaches for producing CP XUV radiation pulses can be found in the literature ([29–31] and references therein) but all campaigns so far have led only to moderate pulse energies.

Nowadays, table-top laser-driven HHG-based sources offer strategies to generate and manipulate the polarization state of highly elliptical/CP XUV light. A key idea underlying several of these methods is to break the symmetry of the system (i.e., to either break the symmetry of the emitting medium or the symmetry of the driving field) [32–34]. Experimental approaches proposed for the generation of CP XUV radiation involve the exploitation of crossed driving laser beams [35], resonant HHG in elliptical laser fields [36], orthogonally-polarized two-color laser fields [37], bichromatic counter-rotating elliptically polarized drivers [38], circularly polarized counter-rotating fields [39–41], or co-rotating bichromatic laser fields [42]. In particular, by implementing counter rotating $\omega/2\omega$ laser fields, an innovative experimental work in 1995 reported the generation of polarization-dependent high-order harmonics [43]. In this case, the polarization state of the higher order harmonics can be fully controlled without significantly reducing the conversion efficiency of the HHG process [33,34]. The generated HHG spectrum then results in the generation

of pairs of harmonics with opposite helicity. The spectral location of the harmonic orders depends on the wavelength of the fundamental and the second harmonic components. The synthesized driving laser field exhibits a threefold spatiotemporal symmetry. Hence, the $3n$ -order (where n is a positive integer) harmonics are forbidden in isotropic media, as in the case of an atomic gas phase medium [39,40,44]. The helicity of the $3n+1$ and $3n-1$ harmonics are the same as those of the fundamental and second harmonic, respectively, and are opposite to each other due to the conservation of spin angular momentum. With respect to the time domain, the electric field resulted by the superposition of the harmonics synthesizes an attosecond pulse train in which each pulse is linearly polarized and the polarization axis rotates by 120° from pulse to pulse [33,41,45].

While the existing literature on the generation of highly elliptical or CP XUV radiation is extensive, the energy content of the experimentally generated pulses is so far limited to pJ regimes [34,46], mostly due to the focusing geometry used for the HHG. In this work, we apply a bichromatic counter rotating circularly polarized laser field to drive HHG in Argon (Ar) atoms under loose focusing conditions, demonstrating the production of ~ 100 nJ highly elliptical polarized XUV radiation in the spectral range of ≈ 20 eV.

2. Methods

In producing a bi-circular field for circular polarized HHG a compact MACH-ZEHNDER-LESS for Threefold Optical Virginia spiderwort-like (MAZEL-TOV-like [47]) scheme is used. A schematic illustration of it is sketched in Figure 1. The experimental investigations were carried out exploiting the MW beamline of the Attosecond Science and Technology Laboratory (AST) at FORTH-IESL. The experiment utilizes a 10 Hz repetition rate Ti:Sapphire laser system delivering pulses up to 400 mJ/pulse energy at $\tau_L = 25$ fs duration and a carrier wavelength at 800 nm. The experimental set-up consists of three chambers: the focusing and MAZEL-TOV-like [47] device chamber, the harmonic generation chamber and the detection chamber. All chambers are under vacuum. A laser beam of 3 cm outer diameter and energy of ≈ 20 mJ/pulse is passing through a 3 m focal-length lens with the MAZEL-TOV-like device positioned 1.25 m downstream. The apparatus consists of a beta-phase barium borate crystal (BBO), a calcite plate and a super achromatic quarter waveplate (Figure 1). A fraction of the energy of the linear p-polarized fundamental pulse, is converted into a perpendicular (s-polarized) second harmonic field (410 nm) in a BBO (0.2 mm, cutting angle 29.2° for type I phase matching). The conversion efficiency of the BBO crystal was maximized and it was found $\approx 30\%$. The run-out introduced by the BBO crystal for the SHG of 800 nm was determined to be 38.6 fs. It is noted that by placing the BBO after the focusing lens ensures that the wavefronts of the converging fundamental laser beam are reproduced into that of the second harmonic field. Therefore, the foci (placed close to a pulsed gas jet filled with Ar) of the ω and 2ω fields coincide along the propagation axis. Additionally, the beam passes through a calcite plate at almost normal incidence (AR coated, group velocity delay (GVD) compensation range 310–450 fs), which pre-compensates group delays introduced by the BBO crystal and the super achromatic quarter waveplate. The super achromatic waveplate converts the two-color linearly polarized pump into a bi-circular field, consisting of the fundamental field and its second harmonic, accumulating at the same time a group delay difference of 253 fs between the 410 nm and 800 nm wavelengths. Assuming Gaussian optics, the intensity at the focus for the two components of the bi-circular polarized field is estimated to be $I_\omega \approx I_{2\omega} \approx 1 \times 10^{14}$ W/cm². After the jet, the produced XUV co-propagates with the bicircular driving fields towards a Si plate, which is placed at 75° reducing the p-polarization component of the fundamental and the second harmonic radiation while reflecting the harmonics [48] towards the detection area. Directly after the Si plate, a pair of 5 mm diameter apertures were placed in order to block the outer part of the ω and 2ω beams, while letting essentially the entire XUV through. A 150 nm thick Sn filter is attached to the second aperture, not only for the spectral selection of the XUV radiation, but also to eliminate the residual bicircular field. A calibrated XUV photodiode (XUV PD) was introduced into the beam path in order to measure the XUV

pulse energy. The transmitted beam enters the detection chamber, where the spectral characterization of the XUV radiation takes place. The characterization is achieved by recording the products of the interaction between the XUV generated beam and the gas phase Ar atoms introduced by a pulsed gas jet valve. The electrons produced by the interaction of Ar atoms with the unfocused XUV radiation were detected by a μ -metal shielded time-of-flight (TOF) spectrometer. The spectral intensity distribution of the XUV radiation is obtained by measuring the single-photon ionization photo-electron (PE) spectra induced by the XUV radiation with photon energy higher than the I_p of Ar ($I_{pAr} = 15.76$ eV).

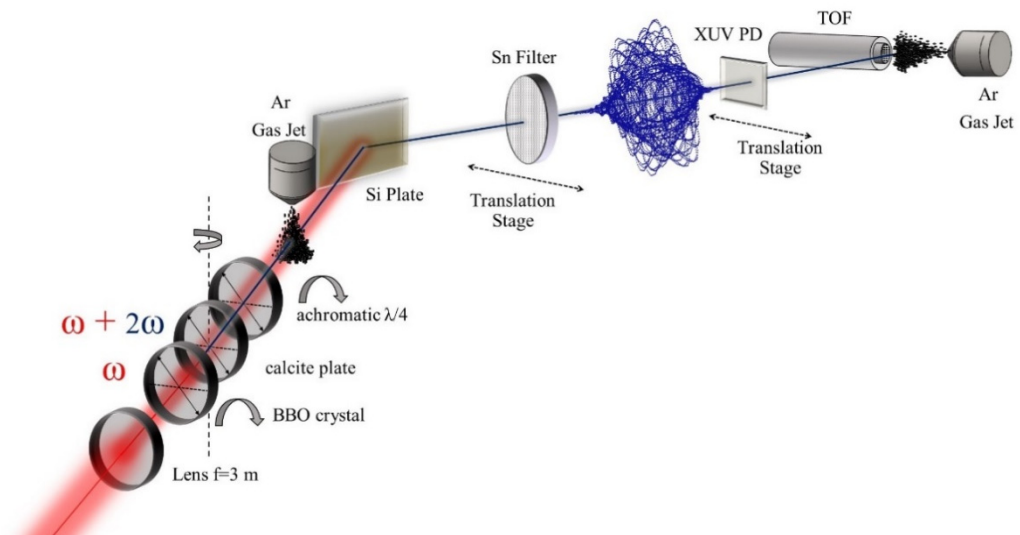


Figure 1. Experimental apparatus for the generation of energetic XUV radiation with the possibility of controllable polarization. A compact (15 cm long) MAZEL-TOV-like device is installed after a 3-m lens. The device includes a BBO crystal, a calcite plate, and a rotatable super achromatic quarter waveplate. The two-color bi-circular field beam is focused into a pulsed gas jet filled with Ar. The generated XUV radiation is reflected towards the detection area by a Si plate. The detection chamber consists of a calibrated XUV photodiode (XUV PD), a pulsed gas jet filled with Ar and finally a μ -metal shielded TOF spectrometer.

3. Results

Exploiting a MAZEL-TOV-like device, the generated HHG spectrum changes from a spectrum which contains only the odd harmonics to a spectrum containing $3n \pm 1$, $n = 1, 2, 3 \dots$ harmonic orders. It is well established in the literature, and verified experimentally and theoretically, that this is a typical spectral signature of highly elliptical polarized HHG radiation in counter rotating $\omega/2\omega$ laser fields [33,34,39–41,45,47]. Figure 2a and the inset show the recorded HHG spectrum of the highly elliptical XUV radiation generated in Ar gas when no metal filter is used. Additionally, Figure 2b shows the spectra of the XUV radiation transmitted through a 150 nm thick Sn filter and the purpose of presenting this spectral region (selected by the Sn filter) is the application of this energetic highly elliptical XUV radiation in two-photon multi-color single or double ionization of rare gases and in relevant circular dichroism experiments in atoms. Although, in this work no ellipsometry measurements have been performed, the presence of highly elliptical XUV radiation is deduced from the appearance of $3n \pm 1$ order harmonics in the spectrum discussed above, as is often the case in similar studies [33,34,47]. Furthermore, it should be noted that other effects that could have resulted these specific observed spectral features have been ruled out. Nonadiabatic short pulse effects at the focus are excluded due to our long driving pulse of 25-fs pulse duration. Any plasma induced frequency shifts of the driver can also be considered being negligible. This is due to the fact that there is lower ionization rate when a bi-chromatic counter rotating circularly polarized laser field interacts with gas phase rare atoms to drive HHG compared to the one of one color

linearly polarized drivers, since the time dependent ellipticity (ϵ) inside the pulse is mostly $\epsilon > 0$ assuming perfect spatiotemporal overlap of these fields. Thus, this results in limited plasma formation. Spectral features originating from the interference between long and short trajectories that can lead to a shift and/or splitting of the harmonic peaks can be also excluded. This is evidenced by the theoretical framework that governs the HHG processes by bicircular polarized fields and detailed analysis of it, which can be found elsewhere [40], based on strong field approximation [49] adapted in the case of bicircular bichromatic driving electric fields and the saddle point analysis (SPA). Here it should be stressed that due to the threefold electric field synthesized by the superposition of the bicircular electric fields, only one trajectory exists during the process of HHG, in contrast to the case of linear monochromatic drivers where two trajectories contribute to harmonic emission [40,41], excluding any quantum phase interference effects.

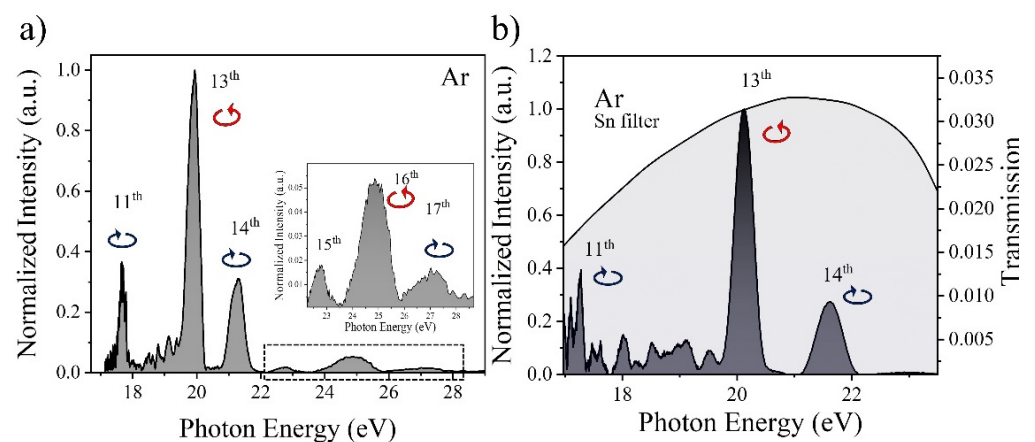


Figure 2. (a) Recorded photoelectron spectrum produced by the interaction of unfiltered highly elliptical polarized XUV radiation with Ar gas. The inset shows a magnified region around harmonic orders 15 to 17; (b) spectrum as in (a) produced by the XUV radiation and transmitted through a 150 nm thick Sn filter.

At this point, as expressed in [50], it should be noted that single photon ionization is a linear process and ionization by highly elliptically polarized fields can be interpreted as the sum of two ionization channels opened by the two perpendicular linearly polarized field of the elliptical laser field. Therefore, the ionization cross section of Argon is assumed to be the same as in the case of linearly polarized light [50]. The red (blue) circular arrow in Figure 2 indicates the rotation direction of the polarization of the fundamental (second harmonic) used for HHG and the transferred helicity to each harmonic.

The highest harmonic order observed was the 17th for Ar exploited as a generating medium. According to the cut-off law, for equal intensities of the ω and 2ω laser field components ($I_\omega = I_{2\omega}$), the highest XUV photon energy emitted is given by the expression: $E_{\max} = 1.2 I_p + \frac{1}{\sqrt{2}} 3.17 U_p$, where $U_p = U_{p\omega} + U_{p2\omega}$ ([34,51,52]). Therefore, in the present experimental conditions the cutoff photon energy is expected to be around the 23rd harmonic. This deviation is attributed to the macroscopic response of the medium and selective phase matching conditions [34,53] which depend on the relative position of the focus of the driving field and the gas jet. Additionally, due to the p character of the ground state of the Ar gas, the harmonics of one helicity are stronger than the harmonics of the opposite one [54]. Finally, the collection efficiency of the TOF spectrometer is lower (compared to the case of linear polarization) when highly elliptical ionizing radiation is applied [55,56], restricting the highest possible observable harmonic orders.

It should be stressed that there is an uncertainty considering the degree of circular polarization of the driving laser shaped by the achromatic quarter waveplate, due to the deviation from an ideal waveplate both in retardation and in the crystal axis. Therefore, the symmetry of the superimposed electric field deviated from the threefold symmetry.

Thus, the 12th and 15th harmonics are still weakly observed in the spectra. The appearance of the $3n$ harmonic orders can be induced by the driving fields' imperfect overlap [57] or by the anisotropy of the generating medium [58,59], a case which is not probable in this experimental investigation since noble gasses are exploited as the generating media and due to the collinear configuration of the MAZEL–TOV like device. Lou Barreau and colleagues [60] showed that by solving the TDSE, breaking can occur (even for perfectly circular driving fields and in an isotropic medium) when the strong-field interaction resulting to the harmonic emission presents sub- ω cycle modulations due to (i) a fast temporal variation of the driving laser fields on the envelope rising and falling edges, causing temporal variations of the harmonic dipole vector and (ii) ionization of the medium, resulting in a fast decay of the induced dipole strength with time.

Moreover, emphasis should be given to the possibility of controlling the harmonic ellipticity and helicity at the source by simply rotating the fast axis of the super achromatic waveplate [33]. This is based on the conservation of spin angular momentum in the HHG process [33]. Considering the formulation described in [33], the equation characterizing the ellipticity for the emitted harmonics allowed by the selection rules (as a function of the angle α of the fast axis of the super achromatic waveplate in the case of a MAZEL–TOV-like device) can be extracted from: $\varepsilon_{n_1, n_2} = \frac{1 - \sqrt{1 - (n_1 - n_2)^2 \sin^2(2\alpha)}}{(n_1 - n_2) \sin(2\alpha)}$ where ε_{n_1, n_2} is the ellipticity of the (n_1, n_2) harmonic channel and $n_2 = n_1 \pm 1$. The equation is valid for an ideal overlap of the two foci and when the generation is by an isotropic medium. Figure 3a presents the estimated harmonic ellipticity ε_{n_1, n_2} as a function of the rotation angle α of the super achromatic waveplate in our MAZEL–TOV-like device installed in the MW beamline of AST at FORTH–IESL. Figure 3b shows the normalized experimental spectra as a function of the angle α of the fast axis of the waveplate in the case of Ar as generating medium. The spectral features demonstrated in Figure 3b can be interpreted theoretically by the model described in [33] and in particular for angles $0^\circ < \alpha < 10^\circ$ (an area out of our interest), were also verified experimentally in [47]. The area for angles $\alpha \geq 40^\circ$ is the desirable area of our studies where it is well known from the literature that represents the generation of highly elliptical radiation in the XUV region. It is also observed that the energy content within this area is approximately the same, with a small deviation (within the experimental error) to the energy measurement discussed in the next subsection.

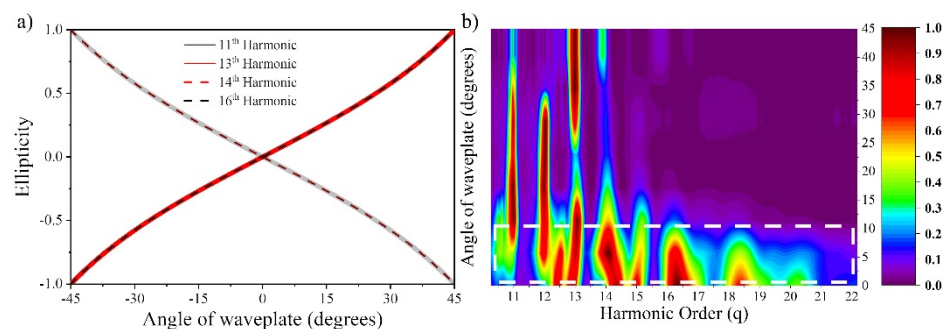


Figure 3. (a) Theoretically predicted ellipticity ε of the 11th, 13th, 14th, 16th harmonics generated in an isotropic medium as a function of the angle α of the super achromatic waveplate's fast axis (see text). (b) Normalized PE spectra as a function of the angle α of the fast axis of the waveplate in the case of Ar.

Energy Content Estimation

The estimation of the energy content of the highly elliptical XUV radiation emitted per pulse is discussed in detail in this section. The estimation is enabled at a first step by measuring the linearly polarized XUV pulse energy by means of the XUV photodiode. Then, by comparing the HHG spectra depicted in the measured photoelectron spectrum of Ar atoms upon interaction with highly elliptically and linearly polarized XUV light, respectively, we can deduce the energy per pulse of the highly elliptical XUV emission.

The linearly polarized HHG signal recorded with the calibrated XUV photodiode (Opto Diode AXUV100G) placed on the XUV beam path after the Sn filter is fed to an oscilloscope with 50Ω input impedance and the measured trace was integrated. In Figure 4a a typical measurement of the p-polarized XUV radiation energy is presented. The photodiode signal was measured with the harmonic generation gas jet ON and OFF. This signal was accumulated for 200 averaged shots. The measured signal when the jet was OFF originates from the residual IR radiation and is subtracted from the signal measured when the generation gas was ON. In this way, one can measure the neat XUV pulse energy. For determining the energy of the harmonic radiation produced at the source one has to consider also the filter transmission as well as the Si reflectivity. Here is the $\sim 3\%$ transmission of the Sn filter in this spectral region measured by recording the harmonic spectrum of linear p-polarized harmonics (with the MAZEL–TOV-like device out of the beam path) with and without filter. The main reason that p-polarized XUV radiation was chosen for the calibration of the Sn filter is the higher signal it results with and without the filter thus minimizing the error of the measurement. The reflectivity of the Si plate is approximately 60% [48]. Under optimal generation conditions, the maximum energies at the source were found to be in the range of $1 \mu\text{J}$. These values concern the emitted 11th, 13th, 15th, 17th, and 19th harmonics laying in the plateau spectral region. Therefore, the energy content per harmonic pulse is $\sim 200 \text{ nJ}$ at the source for Ar.

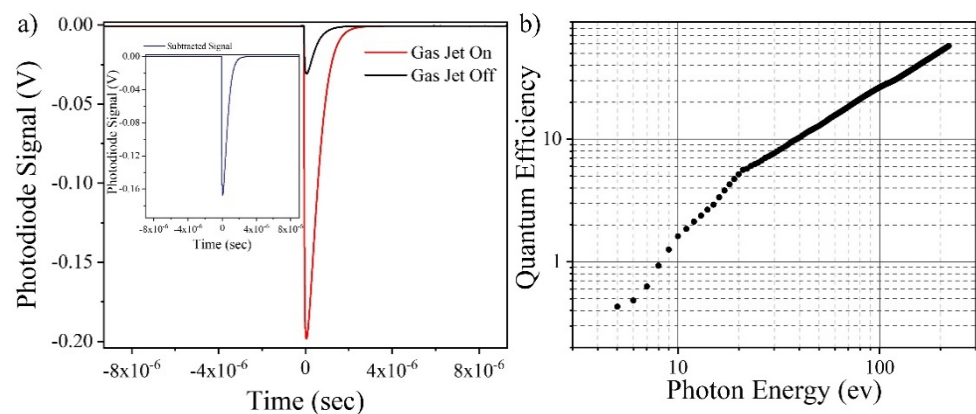


Figure 4. (a) Typical measurement of the p-polarized XUV radiation energy in the case of Ar gas. XUV photodiode signal obtained when HHG switched ON (red line) and with the HHG switched OFF (black line). (b) For the extraction of the pulse energy the XUV photodiode quantum efficiency as a function of photon energy provided by the manufacturing company Opto Diode Corp.

A similar measurement for the highly elliptically polarized radiation has a high degree of uncertainty since the difference of the two signals (gas jet ON—gas jet OFF) is rather small. This is due to the fact that when the MAZEL–TOV-like device is introduced in the beam path, the significantly increased amount of light of the fundamental as well as of the second harmonic frequencies reflected from the Si plate, in the case of non-p-polarized fields, prevents an accurate measurement of the highly elliptical XUV using the XUV PD.

In order to deduce an estimation of the energy per pulse of the highly elliptical XUV light in the present configuration, it is necessary to perform measurements of the Ar single photon ionization PE spectra induced by linear p-polarized and highly elliptical XUV radiation (at the same detection conditions), and directly compare both cases after the optimization of harmonic emission. Figure 5 depicts typical PE spectra in the case of both linear and highly elliptical polarization for Ar gas.

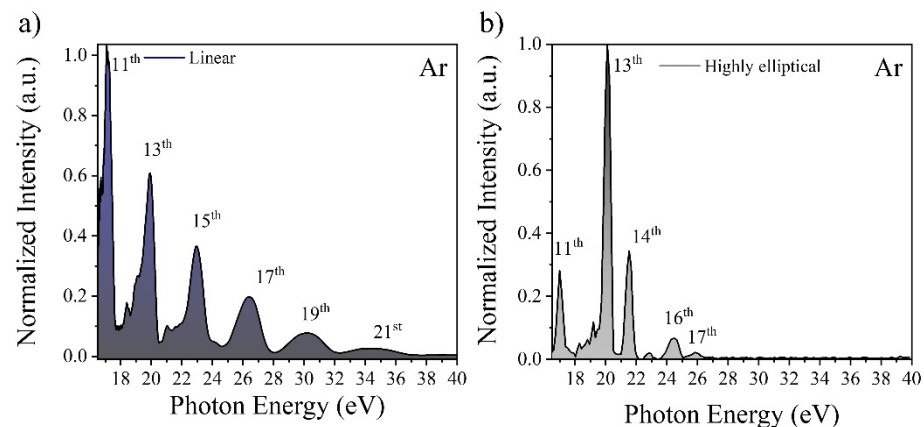


Figure 5. (a) Typical PE spectra of Ar induced by the linear p-polarized and (b) typical highly elliptical XUV radiation generated by Ar at the same detection conditions, as soon as the optimization of harmonic emission is realized in both cases.

Having determined the energy values in the case of linear polarized XUV field and having deduced also the ratios of the harmonic integral values in the case of p-polarization and highly elliptical XUV radiation, by the recordings of the PE spectra, one can extract the energy content of the latter. The typical ratios of the integral values $I_q^{\text{highlyelliptical}} / I_q^{\text{linear}}$, (where q is the harmonic order) deduced from the systematic measurements have been determined for the 11th, 13th, 14th, 16th, and 17th harmonic, respectively, with variations of the order of 50% from day-to-day measurements (within the experimental error). This ratio of the integral values of the two different PE spectra (highly elliptical vs linearly polarized) is equal to the ratio of the energy content of the (per harmonic order) generated XUV radiation. $I_q^{\text{highlyelliptical}} / I_q^{\text{linear}} = E_q^{\text{highlyelliptical}} / E_q^{\text{linear}}$ in both polarizations and has to be divided by the correction parameter ~ 0.6 introduced by the different percentage of the total photoelectrons' number entering the TOF spectrometer. This consideration has to be taken into account due to the different angular photoelectron distributions resulting from the single photon ionization by the two polarization's states (linear, circular) [55,56]. After this correction, the energy per laser pulse emitted in the case of highly elliptical radiation was then estimated to be $E_{Ar}^{\text{highly elliptical}} \approx 100$ nJ. Conclusively, the energy of highly elliptically polarized XUV radiation is ~ 10 times less compared to the linearly polarized XUV radiation at the same spectral region under conditions where the yield was optimized in both cases.

The estimated energy content of $E_{Ar}^{\text{highly elliptical}} \approx 100$ nJ at the source, per driving laser pulse, in conjunction with the implementation of broadband optical elements and tight focusing configurations, is sufficient to induce nonlinear phenomena at the target's area. More specifically, the Si plate used in these experimental investigations can be substituted with custom built multilayers mirrors offering reflectivity up to $\sim 75\%$ in a broad spectral region. A 100 nm thick Al filter can provide transmission of $\sim 80\%$ to the spectral region >17 eV. Finally, a set of gold coated toroidal mirrors, in a Wolter configuration [61] to minimize the coma aberration, can provide high reflectivity ($\sim 80\%$) and a focal spot ~ 3 μm . The combination of the above-mentioned optical elements and arrangements can result in intensity up to $\sim 10^{13}$ W/cm² at the focus.

Reducing the ellipticity of the generated radiation (by varying the fast axis of the super-achromatic waveplate) higher pulse energies were measured. This is a counterplay between the generated energy and the ellipticity of the harmonics.

4. Conclusions

By exploiting the implemented linearly polarized megawatt XUV beamline at FORTH-IESL, we report a method to produce energetic highly elliptical XUV light. The approach is based on gas-phase HHG driven by an intense two-color circularly polarized counter-rotating driving laser field, produced by a MAZEL-TOV-like device when introduced in

the linear MW XUV beamline, under loose focusing conditions. The energy content for the highly elliptical XUV light is deduced by direct comparison between the linear and highly elliptical XUV spectra measured in the photoelectron spectra of Ar atoms (once the energy content of the linearly polarized XUV light is determined). The energy per driving laser pulse in the spectral region between 17 to 26 eV, is found to be in the range of ~100 nJ. Tight focusing of this light in conjunction with appropriately broadband optical elements is anticipated to lead to ~10¹³ W/cm² intensity in the focal area. This intensity would be sufficient to induce nonlinear phenomena in chiral systems in the XUV spectral region.

Author Contributions: Conceptualization, E.V. and E.S.; methodology E.S.; software, E.V. and E.S.; validation, E.S, E.V. and I.O.; formal analysis, E.V. and E.S.; investigation, E.V., E.S. and I.O.; data curation, E.V. and E.S.; writing—original draft preparation, E.V., I.O., I.L. and E.S.; visualization, I.O.; supervision, E.S.; All authors have read and agreed to the published version of the manuscript.

Funding: We acknowledge support of this work by “HELLAS-CH” (MIS Grant No. 5002735) [which is implemented under the “Action for Strengthening Research and Innovation Infrastructures,” funded by the Operational Program “Competitiveness, Entrepreneurship and Innovation” (NSRF 2014–2020) and co-financed by Greece and the European Union (European Regional Development Fund)], the LASERLAB- EUROPE (EU’s Horizon 2020 Grant No. 871124), the IMPULSE project Grant No. 871161), the Hellenic Foundation for Research and Innovation (HFRI) and the General Secretariat for Research and Technology (GSRT) under grant agreements [GAICPEU (Grant No 645)] and NEA-APS HFRI-FM17-2668.

Institutional Review Board Statement: Not applicable.

Informed Consent Statement: Not applicable.

Data Availability Statement: The data presented in this study are available on request from the corresponding author. The data are not publicly available due to privacy.

Conflicts of Interest: The authors declare no conflict of interest.

References

1. Haight, R.; Seidler, P.F. High resolution atomic core level spectroscopy with laser harmonics. *Appl. Phys. Lett.* **1994**, *65*, 517–519. [[CrossRef](#)]
2. Haessler, S.; Caillat, J.; Boutu, W.; Giovanetti-Teixeira, C.; Ruchon, T.; Auguste, T.; Diveki, Z.; Breger, P.; Maquet, A.; Carre, B.; et al. Attosecond imaging of molecular electronic wavepackets. *Nat. Phys.* **2010**, *6*, 200–206. [[CrossRef](#)]
3. Baker, S.; Robinson, J.S.; Haworth, C.A.; Teng, H.; Smith, R.A.; Chirila, C.C.; Lein, M.; Tisch, J.W.G.; Marangos, J.P. Probing Proton Dynamics in Molecules on an Attosecond Time Scale. *Science* **2006**, *312*, 424–427. [[CrossRef](#)]
4. Cavalieri, A.L.; Müller, N.; Uphues, T.; Yakovlev, V.; Baltuška, A.; Horvath, B.; Schmidt, B.; Blümel, L.; Holzwarth, R.; Hendel, S.; et al. Attosecond spectroscopy in condensed matter. *Nat. Cell Biol.* **2007**, *449*, 1029–1032. [[CrossRef](#)] [[PubMed](#)]
5. Sandberg, R.L.; Paul, A.; Raymondson, D.A.; Hädrich, S.; Gaudiosi, D.M.; Holtsnider, J.; Tobey, R.I.; Cohen, O.; Murnane, M.M.; Kapteyn, H.C.; et al. Lensless Diffractive Imaging Using Tabletop Coherent High-Harmonic Soft-X-Ray Beams. *Phys. Rev. Lett.* **2007**, *99*, 098103. [[CrossRef](#)]
6. Miaja-Avila, L.; Saathoff, G.; Mathias, S.; Yin, J.; La-O-Vorakiat, C.; Bauer, M.; Aeschlimann, M.; Murnane, M.M.; Kapteyn, H.C. Direct Measurement of Core-Level Relaxation Dynamics on a Surface-Adsorbate System. *Phys. Rev. Lett.* **2008**, *101*, 046101. [[CrossRef](#)]
7. Li, W.; Zhou, X.; Lock, R.; Patchkovskii, S.; Stolow, A.; Kapteyn, H.C.; Murnane, M.M. Time-Resolved Dynamics in N₂O₄ Probed Using High Harmonic Generation. *Science* **2008**, *322*, 1207–1211. [[CrossRef](#)]
8. Goulielmakis, E.; Loh, Z.-H.; Wirth, A.; Santra, R.; Rohringer, N.; Yakovlev, V.S.; Zherebtsov, S.; Pfeifer, T.; Azzeer, A.M.; Kling, M.F.; et al. Real-time observation of valence electron motion. *Nature* **2010**, *466*, 739–743. [[CrossRef](#)]
9. Seaberg, M.D.; Adams, D.E.; Townsend, E.L.; Raymondson, D.A.; Schlotter, W.F.; Liu, Y.; Menoni, C.S.; Rong, L.; Chen, C.-C.; Miao, J.; et al. Ultrahigh 22 nm resolution coherent diffractive imaging using a desktop 13 nm high harmonic source. *Opt. Express* **2011**, *19*, 22470–22479. [[CrossRef](#)]
10. Mathias, S.; La-O-Vorakiat, C.; Grychtol, P.; Granitzka, P.; Turgut, E.; Shaw, J.; Adam, R.; Nembach, H.T.; Siemens, M.E.; Eich, S.; et al. Probing the timescale of the exchange interaction in a ferromagnetic alloy. *Proc. Natl. Acad. Sci. USA* **2012**, *109*, 4792–4797. [[CrossRef](#)]
11. Hoogeboom-Pot, K.M.; Hernandez-Charpak, J.N.; Gu, X.; Frazer, T.; Anderson, E.H.; Chao, W.; Falcone, R.W.; Yang, R.; Murnane, M.M.; Kapteyn, H.C.; et al. A new regime of nanoscale thermal transport: Collective diffusion increases dissipation efficiency. *Proc. Natl. Acad. Sci. USA* **2015**, *112*, 4846–4851. [[CrossRef](#)]

12. Miao, J.; Ishikawa, T.; Robinson, I.K.; Murnane, M.M. Beyond crystallography: Diffractive imaging using coherent x-ray light sources. *Science* **2015**, *348*, 530–535. [[CrossRef](#)]
13. Zhang, B.; Gardner, D.F.; Seaberg, M.D.; Shanblatt, E.R.; Kapteyn, H.C.; Murnane, M.M.; Adams, D.E. High contrast 3D imaging of surfaces near the wavelength limit using tabletop EUV ptychography. *Ultramicroscopy* **2015**, *158*, 98–104. [[CrossRef](#)] [[PubMed](#)]
14. Skantzakis, E.; Tzallas, P.; Kruse, J.E.; Kalpouzos, C.; Faucher, O.; Tsakiris, G.D.; Charalambidis, D. Tracking Autoionizing-Wave-Packet Dynamics at the 1-fs Temporal Scale. *Phys. Rev. Lett.* **2010**, *105*, 043902. [[CrossRef](#)] [[PubMed](#)]
15. Tzallas, P.; Skantzakis, E.; Nikolopoulos, L.; Tsakiris, G.D.; Charalambidis, D. Extreme-ultraviolet pump–probe studies of one-femtosecond-scale electron dynamics. *Nat. Phys.* **2011**, *7*, 781–784. [[CrossRef](#)]
16. Chatziathanasiou, S.; Lontos, I.; Skantzakis, E.; Kahaly, S.; Kahaly, U.; Tsafrayllis, N.; Faucher, O.; Witzel, B.; Papadakis, N.; Charalambidis, D.; et al. Quantum path interferences in high-order harmonic generation from aligned diatomic molecules. *Phys. Rev. A* **2019**, *100*, 061404. [[CrossRef](#)]
17. Eramo, R.; Cavalieri, S.; Corsi, C.; Lontos, I.; Bellini, M. Method for High-Resolution Frequency Measurements in the Extreme Ultraviolet Regime: Random-Sampling Ramsey Spectroscopy. *Phys. Rev. Lett.* **2011**, *106*, 213003. [[CrossRef](#)] [[PubMed](#)]
18. Takahashi, E.J.; Lan, P.; Mücke, O.D.; Nabekawa, Y.; Midorikawa, K. Attosecond nonlinear optics using gigawatt-scale isolated attosecond pulses. *Nat. Commun.* **2013**, *4*, 2691. [[CrossRef](#)]
19. Fu, Y.; Nishimura, K.; Shao, R.; Suda, A.; Midorikawa, K.; Lan, P.; Takahashi, E.J. High efficiency ultrafast water-window harmonic generation for single-shot soft X-ray spectroscopy. *Commun. Phys.* **2020**, *3*, 92. [[CrossRef](#)]
20. Nayak, A.; Orfanos, I.; Makos, I.; Dumergue, M.; Kühn, S.; Skantzakis, E.; Bodi, B.; Varju, K.; Kalpouzos, C.; Banks, H.I.B.; et al. Multiple ionization of argon via multi-XUV-photon absorption induced by 20-GW high-order harmonic laser pulses. *Phys. Rev. A* **2018**, *98*, 023426. [[CrossRef](#)]
21. Makos, I.; Orfanos, I.; Nayak, A.; Peschel, J.; Major, B.; Lontos, I.; Skantzakis, E.; Papadakis, N.; Kalpouzos, C.; Dumergue, M.; et al. A 10-gigawatt attosecond source for non-linear XUV optics and XUV-pump-XUV-probe studies. *Sci. Rep.* **2020**, *10*, 3759. [[CrossRef](#)]
22. Senfftleben, B.; Kretschmar, M.; Hoffmann, A.; Sauppe, M.; Tümmler, J.; Will, I.; Nagy, T.; Vrakking, M.J.J.; Rupp, D.; Schütte, B. Highly non-linear ionization of atoms induced by intense high-harmonic pulses. *J. Phys. Photon.* **2020**, *2*, 034001. [[CrossRef](#)]
23. Hergott, J.-F.; Kovacev, M.; Merdji, H.; Hubert, C.; Mairesse, Y.; Jean, E.; Breger, P.; Agostini, P.; Carré, B.; Salières, P. Extreme-ultraviolet high-order harmonic pulses in the microjoule range. *Phys. Rev. A* **2002**, *66*, 021801. [[CrossRef](#)]
24. Manschwetus, B.; Rading, L.; Campi, F.; Maclot, S.; Coudert-Alteirac, H.; Lahl, J.; Wikmark, H.; Rudawski, P.; Heyl, C.M.; Farkas, B.; et al. Two-photon double ionization of neon using an intense attosecond pulse train. *Phys. Rev. A* **2016**, *93*, 061402. [[CrossRef](#)]
25. Chatziathanasiou, S.; Kahaly, S.; Skantzakis, E.; Sansone, G.; Lopez-Martens, R.; Haessler, S.; Varju, K.; Tsakiris, G.D.; Charalambidis, D.; Tzallas, P. Generation of Attosecond Light Pulses from Gas and Solid State Media. *Photonics* **2017**, *4*, 26. [[CrossRef](#)]
26. Tzallas, P.; Charalambidis, D.; Papadogiannis, N.; Witte, K.; Tsakiris, G.D. Second-order autocorrelation measurements of attosecond XUV pulse trains. *J. Mod. Opt.* **2005**, *52*, 321–338. [[CrossRef](#)]
27. Nomura, Y.; Hörlein, R.; Tzallas, P.; Dromey, B.; Rykovanov, S.; Major, Z.; Osterhoff, J.; Karsch, S.; Veisz, L.; Zepf, M.; et al. Attosecond phase locking of harmonics emitted from laser-produced plasmas. *Nat. Phys.* **2009**, *5*, 124. [[CrossRef](#)]
28. Hörlein, R.; Nomura, Y.; Tzallas, P.; Rykovanow, S.; Dromey, B.; Osterhoff, J.; Major, Z.; Karsch, S.; Veisz, L.; Zepf, M.; et al. Temporal characterization of attosecond pulses emitted from solid-density plasmas. *New J. Phys.* **2010**, *12*, 043020. [[CrossRef](#)]
29. Schmidt, J.; Guggenmos, A.; Hofstetter, M.; Chew, S.H.; Kleineberg, U. Generation of circularly polarized high harmonic radiation using a transmission multilayer quarter waveplate. *Opt. Express* **2015**, *23*, 33564–33578. [[CrossRef](#)] [[PubMed](#)]
30. Vodungbo, B.; Sardinha, A.B.; Gautier, J.; Lambert, G.; Valentin, C.; Lozano, M.; Iaquaniello, G.; Delmotte, F.; Sebban, S.; Lüning, J.; et al. Polarization control of high order harmonics in the EUV photon energy range. *Opt. Express* **2011**, *19*, 4346–4356. [[CrossRef](#)] [[PubMed](#)]
31. Zhai, C.; Shao, R.; Lan, P.; Wang, B.; Zhang, Y.; Yuan, H.; Njoroge, S.M.; He, L.; Lu, P. Ellipticity control of high-order harmonic generation with nearly orthogonal two-color laser fields. *Phys. Rev. A* **2020**, *101*, 053407. [[CrossRef](#)]
32. Skantzakis, E.; Chatziathanasiou, S.; Carpeggiani, P.A.; Sansone, G.; Nayak, A.; Gray, D.; Tzallas, P.; Charalambidis, D.; Hertz, E.; Faucher, O. Polarization shaping of high-order harmonics in laser-aligned molecules. *Sci. Rep.* **2016**, *6*, 39295. [[CrossRef](#)]
33. Fleischer, A.; Kfir, O.; Diskin, T.; Sidorenko, P.; Cohen, O. Spin angular momentum and tunable polarization in high-harmonic generation. *Nat. Photon.* **2014**, *8*, 543–549. [[CrossRef](#)]
34. Kfir, O.; Grychtol, P.; Turgut, E.; Knut, R.; Zusin, D.; Popmintchev, D.; Popmintchev, T.; Nembach, H.T.; Shaw, J.M.; Fleischer, A.; et al. Generation of bright phase-matched circularly-polarized extreme ultraviolet high harmonics. *Nat. Photon.* **2015**, *9*, 99–105. [[CrossRef](#)]
35. Hickstein, D.D.; Dollar, F.J.; Grychtol, P.; Ellis, J.L.; Knut, R.; Garcia, C.H.; Zusin, D.; Gentry, C.; Shaw, J.M.; Fan, T.; et al. Non-collinear generation of angularly isolated circularly polarized high harmonics. *Nat. Photon.* **2015**, *9*, 743–750. [[CrossRef](#)]
36. Ferré, A.; Handschin, C.; Dumergue, M.; Burgy, F.; Comby, A.; Descamps, D.; Fabre, B.; Garcia, G.; Généaux, R.; Merceron, L.; et al. A table-top ultrashort light source in the extreme ultraviolet for circular dichroism experiments. *Nat. Photon.* **2015**, *9*, 93–98. [[CrossRef](#)]
37. Lambert, G.; Vodungbo, B.; Gautier, J.; Mahieu, B.; Malka, V.; Sebban, S.; Zeitoun, P.; Lüning, J.; Perron, J.; Andreev, A.; et al. Towards enabling femtosecond helicity-dependent spectroscopy with high-harmonic sources. *Nat. Commun.* **2015**, *6*, 6167. [[CrossRef](#)] [[PubMed](#)]

38. Fleischer, A.; Sidorenko, P.; Cohen, O. Generation of high-order harmonics with controllable elliptical polarization. *Opt. Lett. OSA* **2013**, *38*, 223–225. [[CrossRef](#)] [[PubMed](#)]
39. Long, S.; Becker, W.; McIver, J.K. Model calculations of polarization-dependent two-color high-harmonic generation. *Phys. Rev. A* **1995**, *52*, 2262–2278. [[CrossRef](#)] [[PubMed](#)]
40. Milošević, D.B.; Becker, W.; Kopold, R. Generation of circularly polarized high-order harmonics by two-color coplanar field mixing. *Phys. Rev. A* **2000**, *61*, 063403. [[CrossRef](#)]
41. Milošević, D.B.; Becker, W. Attosecond pulse trains with unusual nonlinear polarization. *Phys. Rev. A* **2000**, *62*, 011403. [[CrossRef](#)]
42. Bandrauk, A.D.; Guo, J.; Yuan, K.-J. Circularly polarized attosecond pulse generation and applications to ultrafast mag-netism. *J. Opt.* **2017**, *19*, 124016. [[CrossRef](#)]
43. Eichmann, H.; Egbert, A.; Nolte, S.; Momma, C.; Wellegehausen, B.; Becker, W.; Long, S.; McIver, J.K. Polarization-dependent high-order two-color mixing. *Phys. Rev. A* **1995**, *51*, R3414–R3417. [[CrossRef](#)]
44. Möller, M.; Cheng, Y.; Khan, S.D.; Zhao, B.; Zhao, K.; Chini, M.; Paulus, G.G.; Chang, Z. Dependence of high-order-harmonic-generation yield on driving-laser ellipticity. *Phys. Rev. A* **2012**, *86*, 011401. [[CrossRef](#)]
45. Fan, T.; Grychtol, P.; Knut, R.; Hernández-García, C.; Hickstein, D.D.; Zusin, D.; Gentry, C.; Dollarm, F.; Mancuso, C.; Hogle, C.W.; et al. Bright circularly polarized soft X-ray high harmonics for X-ray magnetic circular dichroism. *Proc. Natl. Acad. Sci. USA* **2015**, *112*, 14206–14211. [[CrossRef](#)] [[PubMed](#)]
46. Comby, A.; Bloch, E.; Beauvarlet, S.; Rajak, D.; Beaulieu, S.; Descamps, D.; Gonzalez, A.; Guichard, F.; Petit, S.; Zaouter, Y.; et al. Bright, polarization-tunable high repetition rate extreme ultraviolet beamline for coincidence electron–ion imaging. *J. Phys. B At. Mol. Opt. Phys.* **2020**, *53*, 234003. [[CrossRef](#)]
47. Kfir, O.; Bordo, E.; Haham, G.I.; Lahav, O.; Fleischer, A.; Cohen, O. In-line production of a bi-circular field for generation of helically polarized high-order harmonics. *Appl. Phys. Lett.* **2016**, *108*, 211106. [[CrossRef](#)]
48. Takahashi, E.J.; Hasegawa, H.; Nabekawa, Y.; Midorikawa, K. High-throughput, high-damage-threshold broadband beam splitter for high-order harmonics in the extreme-ultraviolet region. *Opt. Lett.* **2004**, *29*, 507. [[CrossRef](#)] [[PubMed](#)]
49. Lewenstein, M.; Balcou, P.; Ivanov, M.Y.; L’Huillier, A.; Corkum, P. Theory of high harmonic generation by low-frequency laser fields. *Phys. Rev. A* **1994**, *49*, 2117–2132. [[CrossRef](#)]
50. Majety, V.P.; Scrinzi, A. Photo-Ionization of Noble Gases: A Demonstration of Hybrid Coupled Channels Approach. *Photonics* **2015**, *2*, 93–103. [[CrossRef](#)]
51. Milošević, D.B.; Becker, W.; Kopold, R.; Sandner, W. High-harmonic generation by a bichromatic bicircular laser field. *Laser Phys.* **2001**, *11*, 165–168.
52. Hasović, E.; Becker, W.; Milošević, D.B. Electron rescattering in a bicircular laser field. *Opt. Express* **2016**, *24*, 6413–6424. [[CrossRef](#)]
53. Kfir, O.; Grychtol, P.; Turgut, E.; Knut, R.; Zusin, D.; Fleischer, A.; Bordo, E.; Fan, T.; Popmintchev, D.; Popmintchev, T.; et al. Helicity-selective phase-matching and quasi-phase matching of circularly polarized high-order harmonics: Towards chiral attosecond pulses. *J. Phys. B At. Mol. Opt. Phys.* **2016**, *49*, 123501. [[CrossRef](#)]
54. Milosevic, D.B. Generation of elliptically polarized attosecond pulse trains. *Opt. Lett.* **2015**, *40*, 2381–2384. [[CrossRef](#)] [[PubMed](#)]
55. Cui, H.-F.; Miao, X.-Y. Photoelectron momentum distributions of single-photon ionization under a pair of elliptically polarized attosecond laser pulses. *Chin. Phys. B* **2020**, *29*, 074203. [[CrossRef](#)]
56. Reid, K.L. Photoelectron Angular Distributions. *Annu. Rev. Phys. Chem.* **2003**, *54*, 397–424. [[CrossRef](#)] [[PubMed](#)]
57. Jiménez-Galán, A.; Zhavoronkov, N.; Schloz, M.; Morales, F.; Ivanov, M. Time-resolved high harmonic spectroscopy of dynamical symmetry breaking in bi-circular laser fields: The role of Rydberg states. *Opt. Expr.* **2017**, *25*, 22880–22896. [[CrossRef](#)]
58. Baykusheva, D.; Ahsan, M.; Lin, N.; Wörner, H. Bicircular High-Harmonic Spectroscopy Reveals Dynamical Symmetries of Atoms and Molecules. *Phys. Rev. Lett.* **2016**, *116*, 123001. [[CrossRef](#)]
59. Yuan, K.-J.; Bandrauk, A.D. Symmetry in circularly polarized molecular high-order harmonic generation with intense bicircular laser pulses. *Phys. Rev. A* **2018**, *97*, 023408. [[CrossRef](#)]
60. Barreau, L.; Veyrinas, K.; Gruson, V.; Weber, S.J.; Auguste, T.; Hergott, J.-F.; Lepetit, F.; Carré, B.; Houver, J.-C.; Doweck, D.; et al. Evidence of depolarization and ellipticity of high harmonics driven by ultrashort bichromatic circularly polarized fields. *Nat. Commun.* **2018**, *9*, 4727. [[CrossRef](#)]
61. Wolter, H. Spiegelsysteme streifenden Einfalls als abbildende Optiken für Röntgenstrahlen. *Ann. Phys.* **1952**, *445*, 94–114. [[CrossRef](#)]